

Ξ^* Resonances in Ξ^- Be Interactions

II. Properties of $\Xi(1820)$ and $\Xi(1960)$ in the $\Lambda\bar{K}^0$ and $\Sigma^0\bar{K}^0$ Channels*

S.F. Biagi^{6,a}, M. Bourquin³, R.M. Brown⁷, H.J. Burckhart^{4,b}, P. Extermann³, M. Gailloud⁵, C.N.P. Gee⁷, W.M. Gibson¹, P. Jacot-Guillarmod⁵, J. Perrier³, K.J. Ragan³, Ph. Rosselet⁵, P. Schirato^{3,c}, H.W. Siebert⁴, V.J. Smith¹, K.P. Streit^{2,4}, J.J. Thresher⁷, A.T. Wood¹, C. Yanagisawa^{7,d}

¹ H.H. Wills Physics Laboratory, University of Bristol, Bristol BS8 1TL, UK

² CERN, CH-1211 Geneva 23, Switzerland

³ University of Geneva, CH-1211 Geneva 4, Switzerland

⁴ Physikalisches Institut, University of Heidelberg, D-6900 Heidelberg, Federal Republic of Germany

⁵ University of Lausanne, CH-1015 Lausanne, Switzerland

⁶ Queen Mary College, University of London, London E1 4NS, UK

⁷ Rutherford Appleton Laboratory, Chilton Didcot OX11 0QX, UK

Received 28 November 1986

Abstract. In an experiment at the CERN-SPS charged hyperon beam, we have investigated the inclusive $\Lambda\bar{K}^0$ and $\Sigma^0\bar{K}^0$ final states formed in Ξ^- Be interactions. In the $\Lambda\bar{K}^0$ channel, we observe a signal at 1826 MeV/c² which can be identified with the known $\Xi(1820)$ resonance. We determine its mass and width to be: $M = 1826 \pm 4$ MeV/c², $\Gamma = 12 \pm 14$ MeV/c². A moment analysis is consistent with a spin of $\frac{3}{2}$ and indicates a negative parity for this spin assignment. Also in the $\Lambda\bar{K}^0$ channel, we observe a 3.6σ signal with the following parameters: $M = 1963 \pm 5$ MeV/c², $\Gamma = 25 \pm 15$ MeV/c². This state, which we call $\Xi(1960)$, is not observed in the $\Sigma^0\bar{K}^0$ channel, leading to an upper limit on the ratio of partial widths $\Sigma\bar{K}/\Lambda\bar{K}$ of 2.3 (90% confidence level). A moment analysis of the $\Lambda\bar{K}^0$ final state indicates a spin of $\frac{5}{2}$ or greater in the natural spin-parity series $\frac{5}{2}^+$, $\frac{7}{2}^-$, etc.

1. Introduction

Available information on strangeness $S = -2$ baryon (Ξ^*) spectroscopy is sparse, in spite of considerable experimental effort. Bubble chamber experiments of

* Work supported in part by the U.K. Science and Engineering Research Council, the Swiss National Foundation for Scientific Research, and the Bundesministerium für Forschung und Technologie, Federal Republic of Germany,

^a Now at University of Liverpool, UK

^b Now at CERN, Geneva, Switzerland

^c Now at Hôpital Cantonal Universitaire, Geneva, Switzerland

^d Now at State University of New York at Stony Brook, USA

the 60's and 70's studying K^- -nucleon interactions were able to identify some Ξ^* states, but were hindered by the small production cross-sections and by the complicated topologies of the final states. Indeed, the number of established Ξ^* states below 2 GeV/c² [1] is still far smaller than expected from quark models (see for example [2]), and different determinations of the parameters of the states (mass and width) are often conflicting. Furthermore, a complete spin-parity determination has only been possible for the $\Xi(1530)$. Using the CERN-SPS charged hyperon beam we have carried out an experiment dedicated to the study of Ξ^* and Ω^* states produced in Ξ^- -Be interactions. In previous publications we have reported on the observation of Ω^* resonances decaying into $\Xi^- \pi^+ K^-$ [3] and on the diffractive production of Ξ^* resonances in the ΛK^- and $\Xi^- \pi^+ \pi^-$ channels [4]. Here we present the results of an analysis of the $\Lambda\bar{K}^0$ inclusive channel.

The plan of this paper is the following: in Sect. 2 we describe the experimental apparatus. Sect. 3 is devoted to the event selection, Sect. 4 to the $\Lambda\bar{K}^0$ effective mass distributions, and Sect. 5 to the angular distributions. In Sect. 6 we consider the $\Sigma^0\bar{K}^0$ final state, and Sect. 7 is devoted to the discussion and conclusion. In the Appendix we briefly outline the moment method used in Sect. 5.

2. The Experimental Apparatus

A detailed description of the CERN-SPS charged hyperon beam has been published elsewhere [5]. The

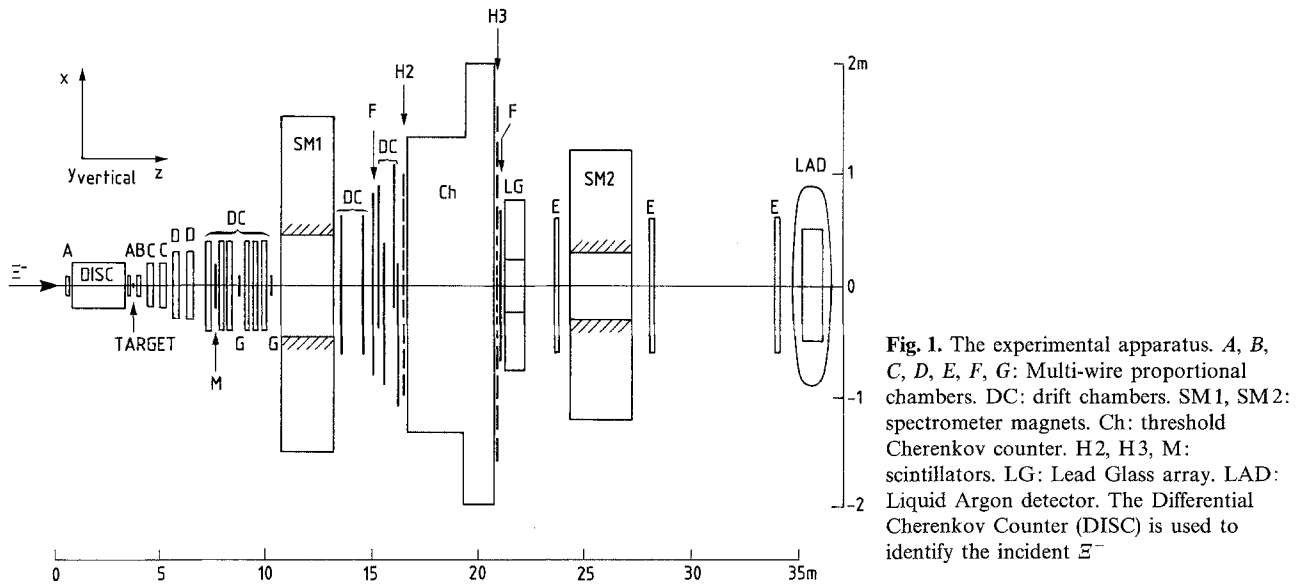


Fig. 1. The experimental apparatus. *A, B, C, D, E, F, G*: Multi-wire proportional chambers. DC: drift chambers. SM1, SM2: spectrometer magnets. Ch: threshold Cherenkov counter. H2, H3, M: scintillators. LG: Lead Glass array. LAD: Liquid Argon detector. The Differential Cherenkov Counter (DISC) is used to identify the incident Ξ^- .

experimental apparatus included a magnetic spectrometer, a threshold Cherenkov counter for π/K separation, and two neutral particle detectors, and is also described in detail elsewhere [3, 6]. Here we briefly recall the parts relevant to the present analysis.

The incident Ξ^- hyperons of mean momentum 116 GeV/c were identified by a differential Cherenkov counter (DISC) and the horizontal and vertical projections of their trajectories measured in two clusters of multi-wire proportional chambers (MWPCs), labelled *A* in Fig. 1. The target was an 83 mm long beryllium rod corresponding to 0.20 nuclear interaction lengths. Trajectories and momenta of outgoing charged particles were measured in a magnetic spectrometer consisting of two magnets (SM1, SM2) and clusters of MWPCs (*B, C, D, E, F, G*) and drift chambers (DC). Upstream of SM1, three independent coordinates at 120° to each other were measured. In the region downstream of SM1 where topologies were less complicated, only two orthogonal coordinates were measured. The gas threshold Cherenkov counter (Ch) provided π/K separation with a nominal π threshold of 10 GeV/c. The Cherenkov and its associated hodoscope H3 were segmented into 24 cells. The lead glass array (LG) and the liquid argon detector (LAD) were used to measure impact points and energies of photons resulting from π^0 and Σ^0 decays. For photon energies above 2 GeV, the normalized LG energy resolution $\sigma(E)/E$ was $0.25/\sqrt{E}$ and that of the LAD was $0.20/\sqrt{E}$ (E in GeV). The spatial resolution of the LG for electromagnetic showers was $13.5/\sqrt{E}$ (mm) and that of the LAD was 3 mm.

A very open trigger was used, demanding only an incident Ξ^- (defined by beam scintillators and the

DISC), at least two charged particles in the multiplicity counter (*M*), and at least three charged particles in at least two different cells of the hodoscope H2. The position of *M* was chosen to allow a 4-metre decay region for secondary hyperons and a sufficient lever arm upstream of SM1 for an accurate momentum measurement of the decay products.

In a typical SPS burst of 1.2 s effective spill time, the beam flux was $1.5 \cdot 10^6$ particles (mostly π^-), the DISC identified approximately 270 Ξ^- , and approximately 60 events fulfilled the trigger conditions. Our total data sample consists of $18 \cdot 10^6$ triggers, corresponding to $82 \cdot 10^6$ DISC-identified Ξ^- .

3. Reconstruction and Event Selection

The longitudinal position of the main interaction vertex was determined using the information from the four MWPCs immediately downstream of the target and the measured incident Ξ^- trajectory. A track reconstructed in the region downstream of the target was considered to be “attached” to this vertex if the distance between the track and the incident Ξ^- trajectory at the position of the vertex was less than 1.5 mm.

Among tracks not attached to the vertex, V^0 candidates were identified if the tracks of two particles of opposite charge intersected downstream of the target with a closest distance of approach (CDA) of less than 3.0 mm. The effective mass of the two secondary particles (assumed to be a proton and a π^-) was then computed. A Λ signal of width 4 MeV/c² (FWHM) was observed, and Λ candidates were accepted if the $p\pi^-$ effective mass was within 8 MeV/c² of the nominal Λ mass; this selection criterion retained

$9.0 \cdot 10^5$ events. Even with this wide mass cut, background under the Λ signal was less than 10% (this background was further reduced using a kinematic fit procedure and an associated χ^2 -probability cut described below).

We next rejected $\Xi^-(\Omega^-)$ inclusive final states by imposing a cut on the $\Lambda\pi^-$ (ΛK^-) effective mass of all combinations of the Λ with additional negative particles, at ± 20 MeV/c² from the nominal $\Xi^-(\Omega^-)$ mass.

A second vee was then demanded. In order to exclude events with two Λ , the proton mass was assigned to the positive particle and the $p\pi^-$ effective mass was required to be larger than 1125 MeV/c². The $\pi^+\pi^-$ effective mass distribution of the second vee had a very clear K_s^0 signal of width (FWHM) 10 MeV/c² above a background of approximately 10% (again, this background was further reduced with a kinematic fit procedure and a χ^2 probability cut). This effective mass was required to be within 15 MeV/c² of the nominal K_s^0 mass; after this selection our sample contained 11,787 events with 11,851 ΛK_s^0 combinations.

The strangeness assignment of the final state is ambiguous because the K_s^0 may be a K^0 or a \bar{K}^0 . We expect that the majority are indeed \bar{K}^0 (strangeness $S = -1$) because the incident particle has $S = -2$ and the cross section for the production of additional units of strangeness will be small, compared to the cross section for production of a system of strangeness $S = -2$ [7, 8]. If the neutral kaon is a K^0 then the strangeness of the identified final state is $S = 0$, and we expect to find additional particles of $S = -1$ in a large proportion of the events. These particles may be baryons but will most likely be kaons; i.e. K^- or \bar{K}^0 . We have already seen that less than 1% of the events satisfying our initial ΛK_s^0 event selection criteria contain two K_s^0 candidates. We have also looked for K^- candidates in our sample, demanding that their momentum be above 12 GeV/c (the position of this cut is dictated by the Cherenkov efficiency for pions which is $\geq 85\%$ above this momentum), that there be no signal in the appropriate Cherenkov cell, and that the appropriate H3 cell be triggered. We find K^- candidates in approximately 4% of the events. The same selection procedure for positively charged particles results in K^+ candidates in 2% of the events. This sets an upper limit on the pion contamination in the K sample. We conclude that the contamination of $S = 0$ final states in our sample is at most at the level of a few percent. In addition we have studied the effective mass distributions of the neutral kaon and an additional π^+ or π^- . In the $K\pi^-$ distribution a very clear $\bar{K}(892)$ signal is visible whereas in the $K\pi^+$ distribution no excess is visible

in the region of the $K(892)$. Because the charge of a charged kaon or kaon resonance is an unequivocal indication of its strangeness, this provides further support that the strangeness of the final state is indeed $S = -2$.

In order to improve the $\Lambda\bar{K}^0$ effective mass resolution, both the Λ and the \bar{K}^0 were submitted to kinematic one-constraint (1-C) fits. The χ^2 -probability distributions are flat for probabilities greater than a few percent. We required both χ^2 -probabilities to be larger than 0.05; after these cuts our data sample consisted of 9090 $\Lambda\bar{K}^0$ combinations.

Finally, in order to exclude events with $\Sigma(1385)$, $\bar{K}(892)$ or Σ^0 , we rejected events in which any $\Lambda\pi^-$ effective mass was in the range 1307 to 1467 MeV/c² or any $\bar{K}^0\pi^-$ effective mass was in the range 790 to 994 MeV/c² (these ranges correspond in each case to $\pm 2\Gamma$ from the mean resonance mass, where Γ is the natural width of the resonance). In addition, we rejected events in which any $\Lambda\gamma$ effective mass fell within ± 25 MeV/c² of the nominal Σ^0 mass (these events will be considered in more detail in Sect. 6). Our data sample after these cuts consists of 4192 $\Lambda\bar{K}^0$ combinations.

4. The Effective Mass Distributions

In Fig. 2a we show the $\Lambda\bar{K}^0$ effective mass distribution of the 4192 combinations after the exclusion of events with Σ^* , K^* and Σ^0 . Excesses are visible near 1680, 1750, 1820, 1960 and 2180 MeV/c². The excess near 1680 is contained in one bin with limits of 1670 MeV/c² and 1685 MeV/c². In an analysis of ΛK^- diffractive production [4], we have observed a very clear $\Xi(1690)$ signal with a mass of $1691 \pm 2 \pm 2$ MeV/c². Our excess is not incompatible with this mass and we will not consider this state any further at this time. The $\Xi(1820)$ state decaying to $\Lambda\bar{K}$ is very well known. However, no state has ever been seen in the $\Lambda\bar{K}$ channel in the mass region from 1900 to 2000 MeV/c², although numerous experiments have reported a signal in the $\Xi\pi$ and $\Xi(1530)\pi$ channels. The situation is unclear, however, because the measurements of the mass and width of this signal (called the $\Xi(1940)$ by the Particle Data Group [1]) are often conflicting.

The $\Lambda\bar{K}^0$ threshold is at 1610 MeV/c². For Ξ^* states well above threshold, produced at large values of x ($x = p_{\Lambda\bar{K}}/p_{\text{beam}} \geq 0.5$) where the acceptance of our apparatus is good, the Lorentz transformation to the laboratory system can result in both particles having large momenta. Thus cuts on the laboratory Λ and \bar{K}^0 momenta may be useful to enhance such Ξ^* signals. As an example, a Monte Carlo simulation of decays of a Ξ^* with a mass of 1960 MeV/c² to $\Lambda\bar{K}^0$

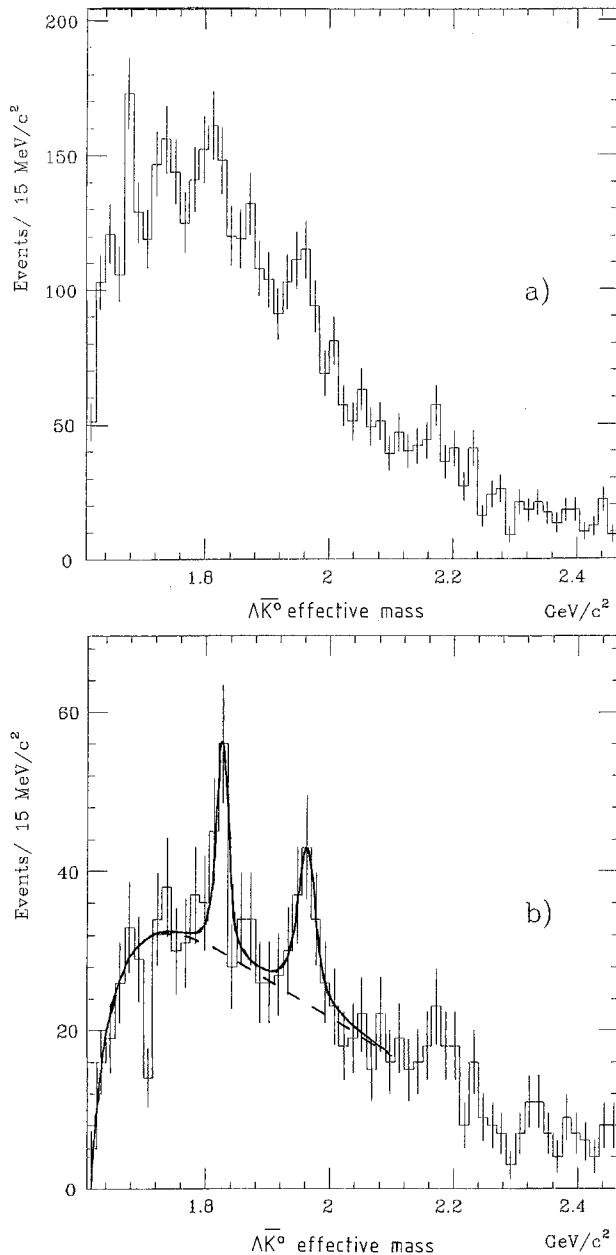


Fig. 2a, b. The $\Lambda\bar{K}^0$ effective mass distribution after $P(\chi^2)$ cuts and removal of Σ^* , \bar{K}^* , and Σ^0 **a**, and after cuts on the kaon and $\Lambda\bar{K}^0$ laboratory momenta **b**. The fit in **b** is described in the text

in our apparatus shows that for Ξ^* momenta above 75 GeV/c ($x=0.65$), only 25% of the decays result in a \bar{K}^0 momentum below 27.5 GeV/c. However in the data sample, 40% of the events having a $\Lambda\bar{K}^0$ momentum above 75 GeV/c have a \bar{K}^0 momentum below 27.5 GeV/c. In Fig. 2b we show the $\Lambda\bar{K}^0$ effective mass distribution for events where the \bar{K}^0 momentum is greater than 27.5 GeV/c and the $\Lambda\bar{K}^0$ momentum is greater than 75 GeV/c. The $\Xi(1820)$ and the structure at 1960 MeV/c² can now be seen very clearly.

The smooth curve in Fig. 2b is the result of an unbinned maximum likelihood fit with a background function plus two Breit-Wigner functions (with the experimental resolution folded in). The background function is a third-order polynomial with an additional term of the form $\sqrt{(m-m_0)}$ where m_0 is the threshold mass; such a term is necessary in order to reproduce the rapid rise of the distribution close to threshold. The resulting Breit-Wigner parameters are:

$$\begin{aligned} M_1 &= 1826 \pm 3 \text{ MeV}/c^2, & \Gamma_1 &= 12 \pm 14 \text{ MeV}/c^2, \\ N_1 &= 54 \pm 17 \text{ events}, \\ M_2 &= 1963 \pm 5 \text{ MeV}/c^2, & \Gamma_2 &= 25 \pm 15 \text{ MeV}/c^2, \\ N_2 &= 63 \pm 24 \text{ events}, \end{aligned}$$

The significances of the signals are estimated by removing each Breit-Wigner in turn and refitting, and then comparing the logarithm of the resulting likelihood to that of the original (and best) fit. The $\Xi(1820)$ signal is found to have a statistical significance of 4.4σ , and the signal at 1963 MeV/c² a significance of 3.6σ . We will henceforth refer to this signal as the $\Xi(1960)$.

The addition of a third Breit-Wigner (again folded with the resolution) to the fit, in the region of the excess seen at 2180 MeV/c², gives a mass and width of: $M=2181 \pm 7 \text{ MeV}/c^2$, $\Gamma=30 \pm 13 \text{ MeV}/c^2$, with 43 ± 11 events in the signal. This signal has a significance of approximately 3σ and may be connected with weak signals we have observed in this mass region in diffractive resonance production in both the $\Lambda\bar{K}^-$ and $\Xi^- \pi^+ \pi^-$ channels [4].

The systematic error on the mass scale has been estimated using the measured masses of the \bar{K}^0 , Λ , Ξ^- , and Ω^- . The systematic errors on the widths of the signals are a result of the uncertainty of approximately 0.5 MeV/c² on the $\Lambda\bar{K}^0$ r.m.s. effective mass resolution (typically 8 MeV/c² in the mass region of interest here), which is a weak function of the momentum of the $\Lambda\bar{K}^0$ system.

Our estimate for the parameters of the two resonances are thus:

$$\begin{aligned} \Xi(1820): & M = 1826 \pm 3 \pm 1 \text{ MeV}/c^2, \\ & \Gamma = 12 \pm 14 \pm 1.7 \text{ MeV}/c^2; \\ \Xi(1960): & M = 1963 \pm 5 \pm 2 \text{ MeV}/c^2, \\ & \Gamma = 25 \pm 15 \pm 1.2 \text{ MeV}/c^2; \end{aligned}$$

where the errors are statistical and systematic, respectively.

The $\Xi(1820)$ is a well-established resonance which has been observed by a number of different experiments in the $\Lambda\bar{K}$, $\Sigma\bar{K}$, and $\Xi(1530)\pi$ channels. The most convincing signal is that of Gay et al. [9] in $\Lambda\bar{K}$. Our results are compatible with their mass and

width determinations ($M = 1823 \pm 2$ MeV/c², $\Gamma = 21 \pm 7$ MeV/c²) and confirm the $\Xi(1820)$ as a narrow state.

The situation in the mass region around 1960 MeV/c² is much less clear. A number of experiments have reported enhancements in this region in the $\Xi\pi$ channel, but the quoted resonance parameters are often conflicting; it is possible that some experiments are observing the superposition of more than one state. No signal in this mass region has ever been convincingly seen in the $\Lambda\bar{K}$ or $\Sigma\bar{K}$ channels. Hassall et al. [10] report a possible excess at 1940 MeV/c² in the $\Sigma^- \bar{K}^0$ mass distribution but see no structure in the $\Sigma^+ K^-$, $\Sigma^0 K^-$, $\Lambda\bar{K}^0$ or ΛK^- channels. Our signal at 1963 MeV/c² is thus the first unequivocal observation of a state in the $\Lambda\bar{K}$ channel in this mass range and it establishes the presence of a relatively narrow resonance in this mass range.

5. Decay Angular Distributions

In order to determine the spin-parity J^P of the resonances discussed in the previous section, we have investigated the angular distributions of the decay chain $\Xi^* \rightarrow \Lambda\bar{K}^0$, $\Lambda \rightarrow p\pi^-$ using a double moment formalism outlined in the Appendix. The double moments $H(lmLM)$ are averages over all events of the product of two Wigner D functions:

$$H(lmLM) \equiv (1/N) \sum_{N \text{ events}} \{D_{Mm}^L(\phi_1, \theta_1) \cdot D_{m0}^L(\phi_2, \theta_2)\},$$

where ϕ_1, θ_1 (ϕ_2, θ_2) are the spherical angles of the Λ (proton) in the center of mass of the $\Xi^*(\Lambda)$. The angles ϕ_2 and θ_2 are measured with respect to the Λ helicity frame.

For $l=1$, odd $L \leq 2J$, and $1 \leq M \leq L$, the ratio of the moments $m=0$ and $m=1$ is related to the spin-parity J^P of the Ξ^* :

$$\text{Im}\{H(11LM)\}/\text{Im}\{H(10LM)\} = P(-1)^{J+1/2} \cdot (2J+1)/\sqrt{2L(L+1)},$$

leading to L independent spin-parity tests for each value of L . Moments with even $L \leq 2J$ may be non-zero but there is no general relation allowing the spin-parity to be determined from them. All moments with $L > 2J$ should be zero.

The cuts applied in the preceding section, as well as any asymmetries in the apparatus, will lead to non-zero values of the moments $H(lmLM)$ even for isotropic decays. We have studied these effects with a Monte Carlo simulation of isotropic decays in our apparatus, applying identical cuts and using distributions of p_L and p_T of the $\Lambda\bar{K}^0$ system which closely resemble the observed distributions. The results show that only

Table 1. The moments $\text{Im}\{H(lmLM)\}$ for $L=1, 3, 5$ for the $\Xi(1960)$. Only the moments used in the spin tests are given here

$m=0$	$m=1$
$L=1$	
$H(1011) = 0.0014 \pm 0.0049$	$H(1111) = -0.0075 \pm 0.0043$
$L=3$	
$H(1033) = 0.0002 \pm 0.0021$	$H(1133) = -0.0016 \pm 0.0012$
$H(1032) = 0.0024 \pm 0.0031$	$H(1132) = -0.0012 \pm 0.0018$
$H(1031) = 0.0090 \pm 0.0092$	$H(1131) = -0.0065 \pm 0.0033$
$L=5$	
$H(1055) = 0.0016 \pm 0.0011$	$H(1155) = 0.0003 \pm 0.0009$
$H(1054) = 0.0007 \pm 0.0012$	$H(1154) = -0.0007 \pm 0.0011$
$H(1053) = 0.0087 \pm 0.0031$	$H(1153) = -0.0019 \pm 0.0013$
$H(1052) = 0.0025 \pm 0.0049$	$H(1152) = 0.0030 \pm 0.0017$
$H(1051) = 0.0093 \pm 0.0118$	$H(1151) = -0.0053 \pm 0.0028$

those moments with $m=0$ or $M=0$ are strongly influenced by these factors. The most strongly affected are the $H(10L0)$ moments, which are only functions of the two polar angles θ_1 and θ_2 ; this is to be expected because the cut on the K^0 momentum creates a forward-backward asymmetry in the Ξ^* centre of mass. Furthermore, we find that only the real parts of the moments are affected ($\text{Im}\{H(10L0)\} \equiv 0$ because of the symmetry of the D functions); these are not in any case used in the spin-parity determination because they must be zero from parity conservation (see Appendix). The imaginary parts of the moments which are used in the spin tests are unaffected by the cuts and the possible asymmetries of the apparatus; all are found to be compatible with zero in the Monte Carlo simulation. In order to check this, we have investigated the moments $H(lmLM)$ up to $L=7$ in the region excluding the observed $\Xi(1820)$ and $\Xi(1960)$ resonances. The imaginary parts of the moments are indeed found to be compatible with zero; statistically their agreement with zero is described by:

$$\chi_L^2 = \sum [\text{Im}\{H(lmLM)\}/\delta \text{Im}\{H(lmLM)\}]^2,$$

where $\delta \text{Im}\{H(lmLM)\}$ represents the statistical uncertainty on the moment $\{H(lmLM)\}$, and where the sum is over the $2L$ independent moments used for the spin tests, for a given value of L . In this region, we find: $\chi_1^2 = 0.6$, $\chi_3^2 = 3.8$, $\chi_5^2 = 11$, and $\chi_7^2 = 8.6$. The corresponding χ^2 -probabilities are 73%, 71%, 34%, and 85% respectively. We thus find no evidence for non-zero imaginary moments outside the resonances.

In the case of the $\Xi(1960)$, we consider the moments in the mass range from 1920 to 2010 MeV/c² (199 events). This choice is a compromise between the signal-to-background ratio which improves as the mass range is tightened around the resonance, and

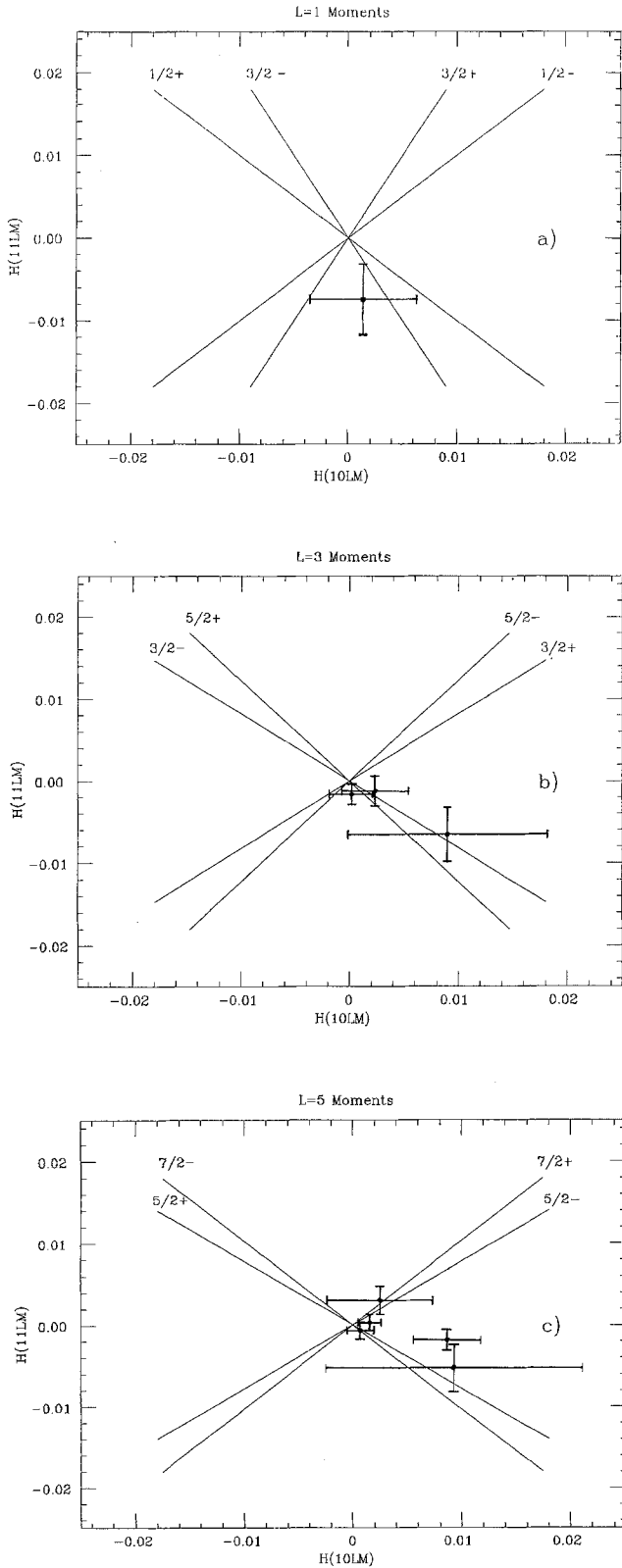


Fig. 3a-c. The moments of the decay sequence $\Xi(1960) \rightarrow A\bar{K}^0$, $A \rightarrow p\pi^-$. **a** $L=1$ moments; **b** $L=3$ moments; **c** $L=5$ moments. In each case the predicted linear relationship of the moments (see text) is also shown, for selected spin-parity values. The numerical values of the moments are given in Table 1

the statistics which become rapidly worse. We have checked that the moments are stable with respect to changes in these cuts. The χ^2_L values that we observe in this region and their probabilities are: $\chi^2_1=3.1$ (21%), $\chi^2_3=7.8$ (25%), $\chi^2_5=20.4$ (3%), $\chi^2_7=16.7$ (27%). Thus the $L=7$ moments are compatible with zero, but we observe non-zero $L=5$ moments (for example, $H(1053)=0.0087 \pm 0.0031$ – a 2.8σ effect). This indicates that the spin of the $\Xi(1960)$ is at least $\frac{5}{2}$, since moments with $L > 2J$ should be zero. The moments for $L=1, 3$, and 5 are given explicitly in Table 1, and shown in Fig. 3, where we plot $H(11LM)$ versus $H(10LM)$. According to the spin test formulated above, these points should fall on straight lines passing through the origin whose slopes are related to L and to the spin-parity J^P of the $\Xi(1960)$. Some of these lines are also plotted in Fig. 3.

Clearly our data shown in Fig. 3 do not allow us to determine uniquely the spin-parity using the moment ratios alone. We have thus combined all the spin tests using the moments with $L \leq 5$ as a single χ^2 test for J^P , using the relation above which relates the moments for $L \leq 2J$ and an expectation value of zero for moments $L > 2J$. The χ^2 -probabilities for spin $\frac{1}{2}$ and $\frac{3}{2}$ are less than 10% because of the non-zero $L=5$ moments. Higher spins in the non-natural spin-parity series $\frac{5}{2}^-$, $\frac{7}{2}^+$, etc., have probabilities of less than 7% and may also be excluded. For the natural spin-parity series $P=(-1)^{J-1/2}$ we find the following probabilities: $\frac{5}{2}^+$: 67%, $\frac{7}{2}^-$: 55%, $\frac{9}{2}^+$: 45%, and thus we cannot distinguish between spins greater than $\frac{3}{2}$. The same test has been performed using the moments up to $L=7$, $L=9$, and $L=11$. In each case, the same features are observed: spins less than $\frac{5}{2}$ and the non-natural spin-parity series have probabilities less than 10% and can be ruled out. Spin-parity $\frac{5}{2}^+$ is preferred (typically with probabilities of 40%), but higher spins in the natural spin-parity series cannot be excluded.

An important test of our moment method is its application to the $\Xi(1820)$, whose spin is known to be $\frac{3}{2}$ [11] and whose parity, although not measured, is believed to be negative [12], in agreement with $SU(3)_{\text{flavour}}$ [13] and quark model [2] predictions. We define the mass region from 1795 to 1855 MeV/ c^2 as our “ $\Xi(1820)$ ” sample (162 events). The signal-to-background ratio here is less favourable than in the $\Xi(1960)$ case, and the non-zero moments are correspondingly less significant. We find: $\chi^2_1=0.2$ (88%), $\chi^2_3=8.4$ (21%), $\chi^2_5=7.5$ (68%), and $\chi^2_7=16$ (31%); i.e. no evidence of non-zero moments for $L \geq 5$. The $L=1$ and $L=3$ moments are shown in Fig. 4. The $L=3$ moments clearly favour $J^P=\frac{3}{2}^-$ compared to $\frac{3}{2}^+$. In order to express this quantitatively, we again reformulate the spin test as a χ^2 test, using the moments with $L \leq 3$. We find that the probability for $\frac{3}{2}^-$ is 94%

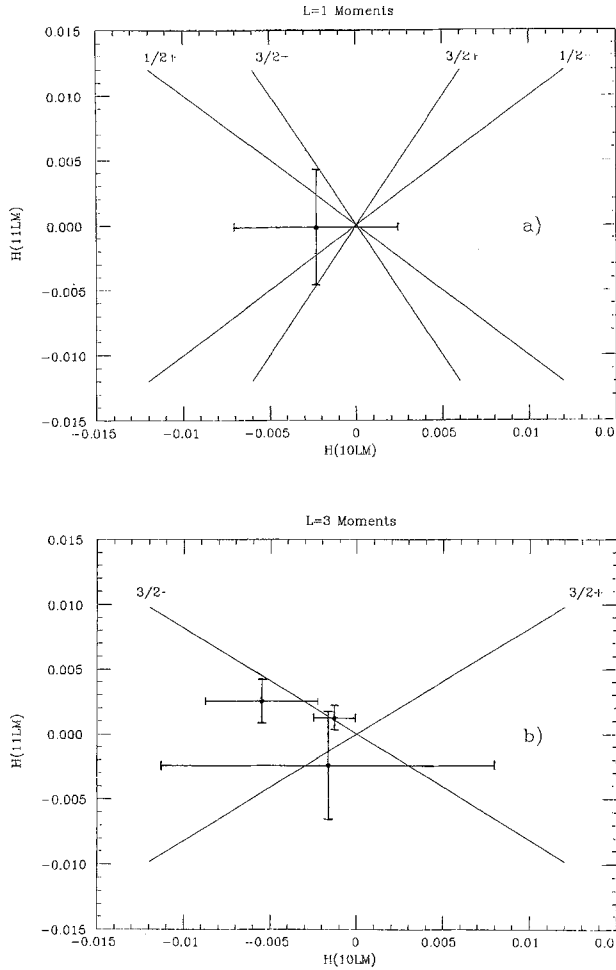


Fig. 4a, b. As in Fig. 3, but for the decay sequence $\Xi(1820) \rightarrow A\bar{K}^0$, $A \rightarrow p\pi^-$

whereas the probability for $\frac{3}{2}^+$ is 9%. Thus, given the $\frac{3}{2}$ spin measurement of Teodoro et al. [11], we unambiguously favor negative parity for the $\Xi(1820)$.

6. The $\Sigma^0 \bar{K}^0$ Channel

The $\Sigma^0 \bar{K}^0$ inclusive channel as observed in our apparatus resembles the $A\bar{K}^0$ channel in many ways. Indeed the similarities of the two states (with one additional γ in the $\Sigma^0 \bar{K}^0$ channel due to the $\Sigma^0 \rightarrow A\gamma$ decay) and their observation in identical experimental conditions permits us to calculate the ratio of branching fractions $R = B(\Sigma \bar{K})/B(A\bar{K})$ of the $\Xi(1960)$ without a detailed knowledge of the Ξ^* production characteristics and the $A\bar{K}^0$ reconstruction efficiency. This ratio is useful for confronting phenomenological models of baryon structure. As an example, the Isgur and Karl model, when applied to the Ξ^* sector [2], predicts eight different states in the mass region from 1900 MeV/c² to 2000 MeV/c². For these states, R

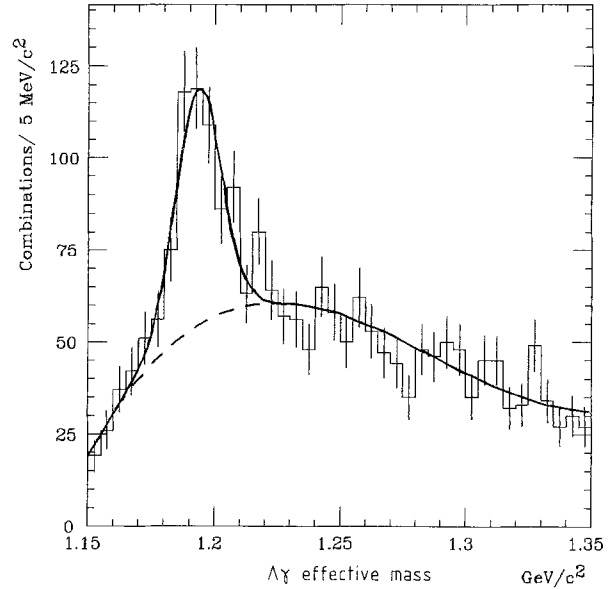


Fig. 5. The $A\gamma$ effective mass spectrum. The fit (smooth curve) is a third-order polynomial with a Gaussian function for the Σ^0 signal

varies from 0.5 to approximately 25, because of the different internal compositions of the states. Clearly, the ratio is a sensitive test of the dynamics of the model.

The initial event sample for this channel is the $A\bar{K}^0$ sample of 9090 combinations obtained after the kinematical fitting procedure and the χ^2 -probability cuts described in Sect. 3. We also remove $\Sigma^*(1385)$ and $\bar{K}^*(892)$ events in the same manner as described there.

Both neutral detectors (the LG array and the LAD) are used to detect photons originating from Σ^0 decays. We reject the data taken during the first 25% of the running time of the experiment, when the efficiencies and calibrations of the neutral detectors were not well understood. Furthermore, we require that the γ energy be greater than 2.5 GeV, because the detection efficiencies of the neutral particle detectors are poorly known for low energy showers. After these cuts we are left with 3058 $A\gamma \bar{K}^0$ combinations in 1924 events.

The $A\gamma$ effective mass distribution for these events is shown in Fig. 5. The fit is a polynomial background (dashed line) plus a Gaussian function with a width of 9.2 MeV/c² (the $A\gamma$ mass resolution of the apparatus at the Σ^0 mass). The fit gives a Σ^0 mass of 1193.4 ± 1.0 MeV/c² with 323 ± 28 events in the signal, in excellent agreement with the accepted value of 1192.5 MeV/c² [1].

We require that the $A\gamma$ effective mass lie within 25 MeV/c² of the nominal Σ^0 mass; this cut reduces our sample to 796 $A\gamma \bar{K}^0$ combinations in 707 events.

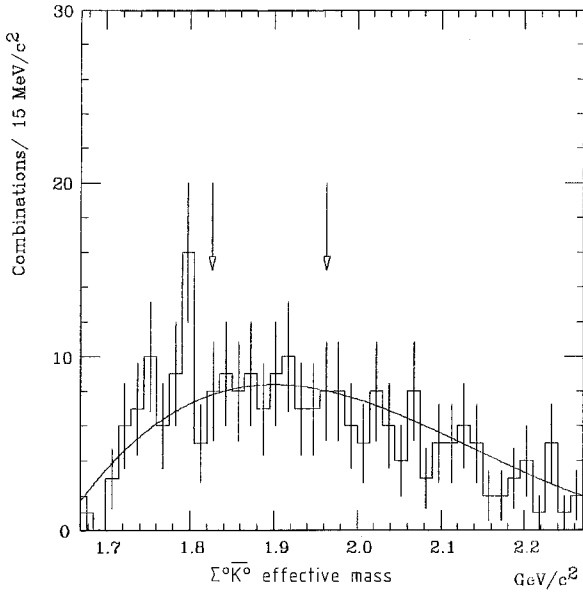


Fig. 6. The $\Sigma^0 \bar{K}^0$ effective mass distribution. No excesses are visible at 1826 or 1963 MeV/c^2 (arrows)

In order to determine the ratio R for the $\Xi(1960)$ using the signal observed in Sect. 4 in the $\Lambda \bar{K}^0$ channel, we apply kinematical cuts similar to those used there. We require the \bar{K}^0 momentum to be greater than $27.5 \text{ GeV}/c$ and the $\Sigma^0 \bar{K}^0$ momentum (i.e. the “ Ξ^* ” momentum) to be greater than $75 \text{ GeV}/c$. After these cuts, the sample contains 265 $\Sigma^0 \bar{K}^0$ combinations in 241 events. The $\Sigma^0 \bar{K}^0$ effective mass distribution for this sample is shown in Fig. 6; there is no excess visible near $1820 \text{ MeV}/c^2$ nor near $1960 \text{ MeV}/c^2$. A one-bin excess is visible at approximately $1795 \text{ MeV}/c^2$, where our experimental resolution (σ) is $10 \text{ MeV}/c^2$. This excess must thus be considered to be a statistical fluctuation.

The smooth curve in Fig. 6 shows the result of a fit with a polynomial background plus a Breit-Wigner signal convoluted with a Gaussian function. The width and central value of the Breit-Wigner are fixed to the values determined above for the $\Xi^0(1960)$, and the width of the Gaussian is fixed to the $\Sigma^0 \bar{K}^0$ mass resolution of the apparatus ($\sigma = 11.5 \text{ MeV}/c^2$). The polynomial background and the number of events in the Breit-Wigner are allowed to vary. The fit gives 0 ± 5 events in the Breit-Wigner, with an upper limit of 11.3 events (90% C.L.).

Using the $\Xi(1960) \rightarrow \Lambda \bar{K}^0$ signal observed in Sect. 4, and taking into account the γ detection efficiency and the slight difference in acceptance in the two channels (caused by the $\Sigma - \Lambda$ mass difference), we find:

$$B[\Xi^0(1960) \rightarrow \Sigma^0 \bar{K}^0]/B[\Xi^0(1960) \rightarrow \Lambda \bar{K}^0] < 0.75 \text{ (90\% C.L.)}$$

The use of identical kinematical cuts in the two channels renders this result independent of any assumptions as to the production characteristics of the $\Xi^0(1960)$, with the proviso that we have not considered spin or polarization effects.

The observation of the $\Xi^0(1960)$ in the $\Lambda \bar{K}^0$ channel leads to an isospin assignment of $I=1/2$. Thus only $1/3$ of the decays $\Xi^0(1960) \rightarrow \Sigma \bar{K}$ are to the $\Sigma^0 \bar{K}^0$ final state, the remainder being to $\Sigma^+ K^-$. Therefore, our limit on the ratio R for the $\Xi(1960)$ becomes:

$$R[\Xi(1960)] = B[\Xi^0(1960) \rightarrow \Sigma \bar{K}]/B[\Xi^0(1960) \rightarrow \Lambda \bar{K}] < 2.3,$$

at the 90% confidence level.

The same method can be used to determine an upper limit for the ratio R for the $\Xi(1820)$. The upper limit on the number of excess events at $1823 \text{ MeV}/c^2$ in Fig. 6 is 14 (90% C.L.), leading to a limit for the ratio R of:

$$R[\Xi(1820)] = B[\Xi^0(1820) \rightarrow \Sigma \bar{K}]/B[\Xi^0(1820) \rightarrow \Lambda \bar{K}] < 3.5,$$

again at the 90% confidence level. This is in agreement with the results of Gay et al. [9], who find a value of 0.24 ± 0.10 .

7. Discussion and Conclusion

We have performed an analysis of the inclusive $\Lambda \bar{K}^0$ final state formed in Ξ^- Be interactions, with selection criteria intended to enhance far-from-threshold resonances. We observe clear signals at $1826 \text{ MeV}/c^2$ and at $1963 \text{ MeV}/c^2$.

The signal at $1826 \text{ MeV}/c^2$ can be identified with the known $\Xi(1820)$ resonance. Our determination of the resonance parameters gives the following results:

$$M[\Xi(1820)] = 1826 \pm 4 \text{ MeV}/c^2, \\ \Gamma[\Xi(1820)] = 12 \pm 14 \text{ MeV}/c^2.$$

These parameters are in good agreement with those of Gay et al. [9] and confirm the $\Xi(1820)$ as a narrow state. An investigation of the decay moments of the $\Xi(1820)$ shows no evidence for non-zero moments for $L > 3$. Given the $\frac{3}{2}$ spin determination of Teodoro et al. [11], our data clearly support the negative parity assignment.

The $\Xi(1820)$ with these properties fits easily into the Isgur and Karl quark model [2] and is also in agreement with $\text{SU}(3)_{\text{flavour}}$ predictions [13].

The signal at $1963 \text{ MeV}/c^2$ represents a 3.6σ effect, and we interpret it as a Ξ^* resonance with the following mass and width:

$$M[\Xi(1960)] = 1963 \pm 5 \text{ MeV}/c^2,$$

$$\Gamma[\Xi(1960)] = 25 \pm 15 \text{ MeV}/c^2.$$

The observation of this signal establishes the presence of at least one narrow resonance in this mass range. The only other signal reported in this mass region is a broad enhancement seen in the $\Xi\pi$ and $\Xi(1530)\pi$ channels, and could very well be a completely different (and much wider) state. It could also be the superposition of our $\Xi(1960)$ with another state (or states) of slightly lower mass, leading to its large apparent width.

With similar kinematic selection criteria in the $\Sigma^0 \bar{K}^0$ channel, we do not observe a $\Xi(1960)$ signal, and determine an upper limit for the ratio of partial widths:

$$B[\Xi^0(1960) \rightarrow \Sigma \bar{K}]/B[\Xi^0(1960) \rightarrow \Lambda \bar{K}] < 2.3 \text{ (90\% C.L.)}.$$

An investigation of the decay moments of the $\Xi(1960)$ reveals non-zero $L=5$ moments at the 2.5σ level, indicating that the spin is at least $\frac{5}{2}$. The natural spin parity sequence $\frac{5}{2}^+, \frac{7}{2}^-, \frac{9}{2}^+ \dots$ is clearly preferred by the data.

Given the 20 to 30 MeV/c² uncertainty* on the mass predictions of Chao et al., the $\Xi(1960)$ can probably be identified with their predicted $\frac{5}{2}^+$ state at 1935 MeV/c² [2]. Indeed, in this harmonic-oscillator quark model, the $\frac{7}{2}^-$ and $\frac{9}{2}^+$ states will be $N=3$ and $N=4$ states respectively (where N is the excitation level of the harmonic oscillator) and will thus be situated 300 to 500 MeV/c² higher in mass. However, the decay model of Koniuk and Isgur [15, 16] which they use to calculate partial decay widths is unsatisfactory, predicting a $\Sigma \bar{K}/\Lambda \bar{K}$ ratio of approximately 7 which is clearly excluded by our upper limit.

Appendix A

In this appendix we will briefly derive the spin test used in Sect. 5, using the helicity formalism. For a more complete treatment we refer the reader to the literature (see for example [6, 17, 18], and references therein). We consider the process:

$$a + b \rightarrow c + \Xi^*, \quad \Xi^* \rightarrow A + \bar{K}, \quad A \rightarrow p + \pi^-. \quad (\text{A1})$$

We describe each particle except the Ξ^* by its spin s and helicity λ ; the spin-parity of the Ξ^* is J^P and its helicity is λ_{Ξ} .

* This uncertainty can be estimated from the mass differences between non-relativistic [2] and relativistic versions [14] of the harmonic-oscillator quark model

The invariant amplitude of the process (A1) may be written as the product of the amplitudes for each step:

$$\mathcal{M} \sim \sum_{\lambda_{\Xi} \lambda_A} \langle \Omega_2 s_p \lambda_p | \mathcal{M}_A | s_A \lambda_A \rangle \langle \Omega_1 s_A \lambda_A | \mathcal{M}_{\Xi} | J \lambda_{\Xi} \rangle \cdot \langle \Omega \lambda_c \lambda_{\Xi} | T | \lambda_a \lambda_b \rangle \quad (\text{A2})$$

where Ω represents the spherical angles of the reaction products in the collision centre of mass, and Ω_1 and Ω_2 represent the spherical angles of the Ξ^* and A decay products respectively, in the centre of mass of the parent. The first two factors describe the A and Ξ^* decays respectively, and the last factor describes the Ξ^* production process. We have summed here over the unobserved helicities of the intermediate states. The first two factors of (A2) are given by the following two-body decay amplitudes:

$$\langle \Omega_2 s_p \lambda_p | \mathcal{M}_A | s_A \lambda_A \rangle = \sqrt{(2s_A + 1)/4\pi} D_{\lambda_A \lambda_p}^{s_A}(\Omega_2) F_{\lambda_p}^{s_A} \quad (\text{A3})$$

$$\langle \Omega_1 s_A \lambda_A | \mathcal{M}_{\Xi} | J \lambda_{\Xi} \rangle = \sqrt{(2J + 1)/4\pi} D_{\lambda_{\Xi} \lambda_A}^{*J}(\Omega_1) F_{\lambda_A}^J \quad (\text{A4})$$

where $D_{m' m}^J$ is the standard rotation matrix [19], and where the ‘‘helicity decay amplitude’’ F_{λ}^J is proportional to the decay matrix element $\langle JM \lambda | \mathcal{M} | JM \rangle$ (M is the z component of the spin J). We have dropped the helicity subscripts referring to the π and the \bar{K} because these particles have spin zero.

The third factor of equation (A2) is the production amplitude of the resonance Ξ^* , and is related to the spin density matrix

$$\rho_{\lambda_{\Xi} \lambda_{\Xi}} \sim \int d\Omega \sum_{\lambda_a \lambda_b \lambda_c} \langle \Omega \lambda_c \lambda_{\Xi} | T | \lambda_a \lambda_b \rangle \langle \Omega \lambda_c \lambda'_{\Xi} | T | \lambda_a \lambda_b \rangle^* \quad (\text{A5})$$

The joint angular distribution $I(\Omega_1, \Omega_2)$ of the decay products is given by the invariant amplitude (A2) squared, summed over the final state helicities (i.e. of the proton and of the particle c), averaged over the initial state helicities λ_a and λ_b , and integrated over the solid angle Ω . Using (A3), (A4) and (A5), one finds:

$$I(\Omega_1, \Omega_2) = (2s_A + 1)(2J + 1)/16\pi^2 \cdot \sum_{\substack{\lambda_{\Xi} \lambda_{\Xi} \\ \lambda_A \lambda'_A \\ \lambda_p}} \rho_{\lambda_{\Xi} \lambda_{\Xi}} \cdot g_{\lambda_p}^{s_A} g_{\lambda_A \lambda'_A}^J \cdot D_{\lambda_{\Xi} \lambda_A}^J(\Omega_1) D_{\lambda_{\Xi} \lambda'_A}^{*J}(\Omega_1) D_{\lambda_A \lambda_p}^{s_A}(\Omega_2) \cdot D_{\lambda'_A \lambda_p}^{*s_A}(\Omega_2) \quad (\text{A6})$$

where

$$g_{\lambda \lambda'}^s = F_{\lambda}^s \cdot F_{\lambda'}^{*s}$$

is a bilinear product of the helicity decay amplitudes F .

The experimental observables used in Sect. 5 are the double moments of the angular distribution given in (A 6):

$$H(lmLM) \equiv \langle D_{Mm}^L(\Omega_1) \cdot D_{m0}^l(\Omega_2) \rangle \\ = \int d\Omega_1 d\Omega_2 \cdot I(\Omega_1, \Omega_2) \cdot D_{Mm}^L(\Omega_1) \cdot D_{m0}^l(\Omega_2) \quad (\text{A } 7)$$

Using the expression (A 6) for the angular distribution $I(\Omega_1, \Omega_2)$ and the following relation involving the product of three D functions:

$$\int d\Omega D_{j_1 m_1}^{j_1}(\Omega) D_{j_2 m_2}^{j_2}(\Omega) D_{j_3 m_3}^{j_3}(\Omega) \\ = 8\pi^2 / (2J_3 + 1) \cdot \langle J_1 j_1 J_2 j_2 | J_3 j_3 \rangle \\ \cdot \langle J_1 m_1 J_2 m_2 | J_3 m_3 \rangle \quad (\text{A } 8)$$

where the factors on the right are standard Clebsch-Gordan vector coupling coefficients [19], the moments H may be expressed as:

$$H(lmLM) = \sum_{\lambda_\Xi \lambda_\Xi'} \rho_{\lambda_\Xi \lambda_\Xi'} \langle J \lambda_\Xi' LM | J \lambda_\Xi \rangle \\ \cdot \sum_{\lambda_A \lambda_A'} g_{\lambda_A \lambda_A'}^J \langle J \lambda_A' Lm | J \lambda_A \rangle \\ \cdot \langle s_A \lambda_A' lm | s_A \lambda_A \rangle \sum_{\lambda_p} g_{\lambda_p \lambda_p}^{s_A} \langle s_A \lambda_p l0 | s_A \lambda_p \rangle. \quad (\text{A } 9)$$

Here we have explicitly separated the three factors which enter into the moments H , in order to make their physical meaning more clear. The first factor is related to the Ξ^* production and is normally called the multipole parameter, written t_{LM}^{*J} . Note that the Clebsch-Gordan coefficient will be zero for $L > 2J$ and hence the moments H will disappear. The second factor describes the decay of the resonance of spin J in terms of the helicity amplitudes g^J . The third and final factor describes the A decay, also in terms of helicity amplitudes. It is related to the A decay parameter α and hence is a known quantity (and, just as important, is non-zero). Again because of the Clebsch-Gordan coefficient, terms with $l > 2s_A$ will disappear.

The orthonormality of the Clebsch-Gordan coefficients may be used to invert (A 9):

$$t_{LM}^{*J} \cdot g_{\lambda_A \lambda_A'}^J \cdot \langle J \lambda_A' Lm | J \lambda_A \rangle \equiv G_{\lambda_A \lambda_A'}(LM) \\ = \sum_l (2l+1)/(2s_A+1) \cdot \langle s_A \lambda_A' lm | s_A \lambda_A \rangle \\ \cdot H(lmLM) \cdot (f_l)^{-1}. \quad (\text{A } 10)$$

Here we have written the third factor of (A 9) simply as f_l . As noted above, it is a known quantity and the moments $H(lmLM)$ are experimental observables. Thus the function G in (A 10) is a measurable quan-

tity, related to the production of the resonance (via the multipole parameter t) and its decay (via the g and the Clebsch-Gordan coefficients). In particular the ratio of two G functions will be independent of the (unknown) multipole parameter, and can be related directly to the spin of the resonance.

It can be shown that for the parity-conserving decay of the Ξ^* , the helicity amplitudes g^J are:

$$g_{++}^J = g_{--}^J = \frac{1}{2}, \quad g_{+-}^J = g_{-+}^J = P(-1)^{J+1/2} \cdot \frac{1}{2}. \quad (\text{A } 11)$$

where we have written the helicity states of the A as “+” for $\lambda_A = \frac{1}{2}$ and as “-” for $\lambda_A = -\frac{1}{2}$. The A decay is not parity conserving and the f_l are more complicated; they are related to the $A \rightarrow p\pi^-$ decay parameter α and for our purposes it is sufficient that f_1 (and thus α) be non-zero.

We can now write explicitly (A 10) for the decay process (A 1):

$$G_{++}(LM) = \frac{1}{2} \cdot H(00LM) + \frac{3}{2} \cdot \langle \frac{1}{2}, \frac{1}{2}, 1, 0 | \frac{1}{2}, \frac{1}{2} \rangle (f_1)^{-1} \\ \cdot H(10LM) = \frac{1}{2} \cdot H(00LM) - \frac{1}{2} \cdot \sqrt{3} \cdot (f_1)^{-1} \\ \cdot H(10LM) \quad (\text{A } 12)$$

$$G_{+-}(LM) = \sqrt{\frac{3}{2}} \cdot (f_1)^{-1} \cdot H(11LM) \quad (\text{A } 13)$$

for arbitrary values of L and M . Parity conservation in the decay of the Ξ^* leads to the following symmetry property of the moments:

$$H(lmLM) = (-1)^{l+L} H(l-mLM),$$

allowing us to write, for odd L (and using (A 10) and (A 11)):

$$G_{+-}(LM)/G_{++}(LM) \\ = P(-1)^{J+1/2} \langle J, -\frac{1}{2}, L, 1 | J, \frac{1}{2} \rangle / \langle J, \frac{1}{2}, L, 0 | J, \frac{1}{2} \rangle. \quad (\text{A } 14)$$

Using Clebsch-Gordan recursion relations, the ratio of coefficients in (A 14) can be shown to be $(2J+1)/\sqrt{2L(L+1)}$, for arbitrary J and odd L . We thus arrive at the final result:

$$H(11LM)/H(10LM) = P(-1)^{J+1/2} \\ \cdot (2J+1)/\sqrt{2L(L+1)}, \quad (\text{A } 15)$$

valid for odd $L \leq 2J$.

For given l and m , there are $2L+1$ different moments $H(lmLM)$. Each is a complex number, so there are $4L+2$ differential real numbers for each L . For the case of $l=1, m=0$, the use of the symmetry of the D functions reduces this to $2L+1$ independent numbers. Parity conservation in the Ξ^* production process, together with the D function symmetries, implies that a further $L+1$ of these numbers should be

zero (parity conservation in the Ξ^* decay process provides no additional constraints), so that there are only L remaining independent non-zero numbers. These may be taken to be $\text{Im}[H(10LM)]$ for $M > 0$. For the case $l=1, m=1$, we again start with $4L+2$ real numbers. Parity conservation in the production process implies that moments with $M=0$ and L odd are zero, reducing the number of possible non-zero numbers to $4L$. Parity conservation in both the production and the decay processes reduces this to L independent numbers which may be non-zero; they are $\text{Im}[H(11LM)]$ for $M > 0$. The ratio of moments in (A15) is thus the ratio of two purely-imaginary numbers and is real.

References

1. Review of Particle Properties, Particle Data Group: Phys. Lett. **170B** (1986)
2. K.T. Chao, N. Isgur, G. Karl: Phys. Rev. **D23**, 155 (1981)
3. S.F. Biagi et al.: Z. Phys. C – Particles and Fields **31**, 33 (1986)
4. S.F. Biagi et al.: Z. Phys. C – Particles and Fields **34**, 15 (1987)
5. M. Bourquin et al.: Nucl. Phys. **B153**, 13 (1979)
6. K.J. Ragan: PhD. thesis, University of Geneva (1986), unpublished
7. S.F. Biagi et al.: Z. Phys. C – Particles and Fields **9**, 305 (1981)
8. S.F. Biagi et al.: Z. Phys. C – Particles and Fields **34**, 187 (1987)
9. J.B. Gay et al.: Phys. Lett. **62B**, 477 (1976)
10. J.K. Hassall et al.: Nucl. Phys. **B189**, 397 (1981)
11. D. Teodoro et al.: Phys. Lett. **77B**, 451 (1978)
12. D.W. Merrill, J. Button-Shafer: Phys. Rev. **167**, 1202 (1968)
13. N.P. Samios, M. Goldberg, B.T. Meadows: Rev. Mod. Phys. **46**, 49 (1974)
14. S. Godfrey, N. Isgur: Phys. Rev. **D23**, 189 (1981); S. Capstick, N. Isgur: University of Toronto preprint UTPT-85-34
15. R. Koniuk, N. Isgur: Phys. Rev. Lett. **44**, 845 (1980)
16. R. Koniuk, N. Isgur: Phys. Rev. **D21**, 1868 (1980)
17. S.U. Chung: CERN 71-8 (1971)
18. N. Byers, S. Fenster: Phys. Rev. Lett. **11**, 52 (1963)
19. M.E. Rose: Elementary theory of angular momentum. Princeton: Princeton University Press 1957